Available online at www.sciencedirect.com
ScienceDirect
International Journal of Thermal Sciences 47 (2008) 324–338
International Journal of Thermal Sciences
www.elsevier.com/locate/ijts

Experimental and theoretical study of the hot-ring method applied to low-density thermal insulators

R. Coquard [a,*,1], D. Baillis [b,2], D. Quenard [a,1]

[a] *Centre Scientifique et Technique du Bâtiment (CSTB), 24 rue Joseph FOURIER, 38400 Saint Martin d'Hères, France*
[b] *Centre Thermique de Lyon (CETHIL), UMR CNRS 5008, Domaine Scientifique de la Doua, INSA de Lyon, Bâtiment Sadi Carnot, 9 rue de la physique, 69621 Villeurbanne CEDEX, France*

Received 13 February 2006; received in revised form 20 December 2006; accepted 16 January 2007

Available online 11 December 2007

Abstract

Among all the transient techniques of measurement of the thermal conductivity, the hot-wire method is an interesting alternative to the standard guarded hot-plate method. However, it has been proved to be poorly adapted to low-density thermal insulators notably due to edge effects, which disturb the temperature rise. To overcome this problem, the hot-ring method, which is very close to the hot-wire technique, could be interesting as it does not make any assumptions on the dimensions of the heating elements. In order to investigate the use of this method for measurements on low-density thermal insulators we conducted a theoretical and experimental study on several expanded polystyrene (EPS) foam samples. The numerical model developed solves the 2-D axisymmetric heat transfer around the ring taking into account the conduction–radiation coupling and the inertia of the element. Numerical and experimental results show that classical hot-ring apparatus are poorly adapted to measurements on low-density insulators owing to the thermal inertia of the elements. However, we developed a modified identification procedure eliminating the influence of the inertia of the apparatus on the measured thermal conductivity. This new procedure gives accurate results even for EPS foams, which could not be considered as optically thick. Thus, the hot-ring technique could be extended to low-density thermal insulators.
© 2007 Elsevier Masson SAS. All rights reserved.

Keywords: Thermal insulator; Thermal conductivity; Hot-ring method; Radiation–conduction coupling; Thermal inertia

1. Introduction

The accuracy of thermal properties measurement takes on particular importance in numerous physical, chemical or medical applications given that it has a direct influence on the estimation of heat losses, or temperature rise. For purely conductive materials, heat transfer is characterized by the basic energy equation and the Fourier law depending on three parameters: the thermal conductivity, the density and the specific heat. Standard measuring methods of these parameters are based on steady state techniques. For the estimation of the thermal conductivity, the principle of the guarded hot plate method is to measure the heat flux passing through a slab of materials subjected to a one-dimensional steady state heat transfer. This technique gives very accurate results. Nevertheless, it is restricting given that the slab must have large and standard dimensions and that it requires especially long measuring durations.

That is the reason why, during the last two decades, there has been a significant development of the transient methods of measurement of thermophysical properties on a broad range of materials. For example, Tan et al. [1], Hahn et al. [2] or Lazard et al. [3] studied the application of the flash method for the measurement of the thermal diffusivity of semi-transparent media in which radiative heat transfer is significant. Lazard et al. [3] proposed a complete methodology to adapt the method to this kind of materials. Nevertheless, the transient method which is the most widely used for the measurement of thermal conductivity is the so-called hot-wire method. Indeed, it is relatively simple and fast as it is based on the transient measurement of the temperature rise of a uniformly heated wire. Moreover,

* Corresponding author.
E-mail addresses: r.coquard@cstb.fr (R. Coquard), dominique.baillis@insa-lyon.fr (D. Baillis).
[1] Tel.: +33 04 76 76 25 53.
[2] Tel.: +33 04 72 43 84 74.

1290-0729/$ – see front matter © 2007 Elsevier Masson SAS. All rights reserved.
doi:10.1016/j.ijthermalsci.2007.01.015

Nomenclature

A	thickness of the kapton slab ..... m
B	thickness of kapton still present around the ring for configuration 3 (see Fig. 4) ..... m
C	specific heat ..... $J\,kg^{-1}\,K^{-1}$
C_p	specific heat of the porous medium .. $J\,kg^{-1}\,K^{-1}$
$g = 0.5\int_{-1}^{1} P(\mu')\mu'\,d\mu'$	asymmetry factor of the phase function
$I(r,z,\theta,\varphi)$	radiant intensity at point (r,z) in the direction (θ,φ) ..... $W\,m^{-2}\,sr^{-1}$
$I^0(T)$	radiant intensity emitted by a black body at temperature T ..... $W\,m^{-2}\,sr^{-1}$
k	thermal conductivity ..... $W\,m^{-1}\,K^{-1}$
k_c	effective or phonic thermal conductivity of the material ..... $W\,m^{-1}\,K^{-1}$
$k_{eq.m}$	equivalent thermal conductivity measured by the guarded hot-plate method ..... $W\,m^{-1}\,K^{-1}$
$k_{eq.th}$	equivalent thermal conductivity computed theoretically for a 1-D steady-state heat transfer ..... $W\,m^{-1}\,K^{-1}$
k_{hot}	thermal conductivity evaluated by the hot-ring method ..... $W\,m^{-1}\,K^{-1}$
n_d	number of directions of the angular discretization
$nR, nZ, n\varphi$	number of spatial discretization along the r, z and φ coordinates respectively
nRm	number of radial discretization for the volume with radius lower than R_r
$n\varphi$	number of discretization of the angle φ
$n\varphi_r$	number of φ discretization occupied by the ring
$P(\nu)$	global scattering phase function
q_c	conductive heat flux ..... $W\,m^{-2}$
q_r	radiative heat flux ..... $W\,m^{-2}$
q_t	total heat flux ..... $W\,m^{-2}$
$\dot{Q}$	heating power ..... W
r	radial coordinate
R	Radius ..... m
t	heating time ..... s
T	temperature ..... K
T_c	temperature at the center of the ring ..... K
V	volume ..... m^3
w_m	weighting factors of the discretization
z	axial coordinate

Greek symbols

β, κ and σ	global extinction, absorption and scattering coefficients ($\beta = \kappa + \sigma$) ..... m^{-1}
σ_{SB}	Stefan–Boltzmann constant ($\approx 5.67 \times 10^{-8}\,W\,m^{-2}\,K^{-4}$)
ε	emissivity
λ	Wavelength of radiation ..... μm
ρ	density of the foam ..... $kg\,m^{-3}$
ρ_r	density of the material constituting the hot-wire ..... $kg\,m^{-3}$
ρ_k	density of the kapton slab ..... $kg\,m^{-3}$
$\eta = \sin\theta.\sin\varphi$	direction cosine
$\mu = \sin\theta.\cos\varphi$	direction cosine along the radial coordinate
$\xi = \cos\theta$	direction cosine along the axial coordinate
(θ, ϕ)	direction angles of the radiant intensity
φ	azimuthal angle
$\nu = \mu.\mu' + \eta.\eta' + \xi.\xi'$	is the cosine of the angle between incident and scattering directions
ψ	angle covered by the ring
$\omega = \sigma/\beta$	scattering albedo
Ω_r	electrical resistance of the ring ..... Ω
Ω	solid angle ..... sr

Subscripts

init	initial
k	of the kapton slab
max	maximal coordinate
r	of the ring
ROSS	from Rosseland approximation

Superscript

r	along the radial coordinate
z	along the axial coordinate

measurements could be made on samples with any shapes and relatively small sizes. It has been used successfully in numerous studies such as [4] for solid and pasty thermal insulators or soil [5] and gives satisfactory results. However, as the method is based on the Fourier diffusion law, it is theoretically not applicable to materials where radiative heat transfer occurs such as low-density thermal insulators.

Coquard et al. [6] have studied theoretically and experimentally the application of this transient techniques to low-density materials where both conductive and radiative transfer are significant. They developed a detailed 2-D simulation of axisymmetric transient heat transfer taking into account the coupling between conduction and radiation, the inertia of the wire, the thermal contact resistance and the edge effects. Simultaneously, they conducted a series of measurements of the thermal conductivity using several hot wire measuring systems on four low-density expanded polystyrene (EPS) foams whose conductive and radiative properties have been previously characterized. The numerical results obtained for these low-density thermal insulators show that once the thermal inertia of the wire becomes negligible, the conductivity of the foams measured by the hot-wire method tends to the equivalent conductivity given by the guarded hot-plate method. Thus, the hot-wire measuring method could theoretically be extended to semi-transparent materials even when they do not behave like optically thick materials (Rosseland approximation). Nevertheless, the experimental and numerical investigations also revealed that classical hot-wire apparatus are poorly adapted to equivalent thermal conductivity measurements on thermal insulators whose density is lower than 30 $kg\,m^{-3}$ given that the maximum length of

classical hot-wires ($L = 0.1$ m) is not sufficiently important to avoid edge effects. Then, relatively long wires should theoretically be used which would lead to a decrease of the interest of the method whose main advantage is the commodity and convenience.

The hot-ring technique is another transient method of measurement of the thermal conductivity. The principle of measurement is very close to that of the hot-wire method except that the heated wire is replaced by a ring at the center of which the temperature rise is measured. This method presents an interest for measurements on low-density materials given that, contrary to the hot-wire method which assumes an infinitely long wire, no assumptions are made on the dimensions of the heated element. However, like the hot-wire method it is based on the assumption of purely conductive medium and could theoretically not be used on materials where radiative heat transfer occurs. In order to determine whether the method could be extended to semi-transparent low-density materials, we conducted a theoretical and experimental study of the hot-ring measurement method applied to low-density EPS foams. At first, we recall the principle of the method and the governing equations for a complete ring with no inertia in a purely conductive medium. Then, we describe the theoretical model developed to take into account the influence of the coupling between conduction and radiation and the inertia of the apparatus on the temperature rise at the center of the ring. The 2-D axisymmetric energy equation and Radiative Transfer Equation are solved numerically. The radiative and conductive properties of the EPS foams studied have been determined in a previous study [7]. Finally, the analysis of experimental and numerical results permits us to conclude on the applicability of this method to measurement on low-density thermal insulators.

2. Governing equations

2.1. Thin complete ring in a purely conductive medium

The principle of the standard transient hot-ring method is to heat a thin circular ring of radius R_r immersed in the sample in order to generate a transient temperature field in the material. The measurement of the temperature rise at the center of the ring allows to determine the heat conductivity of the porous medium. Indeed, if we assume that the properties of the medium are isotropic and independent of the temperature, that there is no thermal resistance at the contact area between the ring and the medium and that the ring has a negligible inertia, the evolution of the temperature at the center is the same as that of a point located at a distance R_r from a continuous point source and can be obtained analytically [8] by:

$$\Delta T_c = \frac{\dot{Q}}{4\pi k_c R_r} \operatorname{erfc}\left(\frac{R_r\sqrt{\rho C_p}}{\sqrt{4k_c t}}\right) \tag{1}$$

According to this formula, it is possible to determine the thermal conductivity k_c of the material from the temperature T_1 and T_2 measured at time t_1 and t_2 at the center of the ring. In practice, as the function erfc could not be inverted analytically, it is necessary to use an identification procedure computing the value of k_c, which permits to best fit the temperature rise at the center of the ring.

2.2. Real ring in a semi-transparent medium

In reality, the inertia of the ring is not negligible and the surrounding material in which the ring is embedded is not necessary a pure thermal conductor. Moreover, in practice, in order to ascertain the well-positioning of the ring and to be able to introduce a thermocouple at the center of the circle, experimental apparatus are made of rings with square cross-section embedded in a slab of kapton (see Fig. 1). This could disturb the heat transfer. That is the reason why we developed a simulation of the axisymmetric transient heat transfer taking into account the inertia of the ring and of the experimental apparatus and the coupling between conductive and radiative heat transfer. This model uses the same methods of resolution of the Energy Equation and of the Radiative Transfer Equation as the model developed in [6] for the modeling of the hot-wire method. Thus, we only give a brief description of the model and of the resolution method in this paper and invite the reader to consult [6] for more details. The model permits to compute the temperature in the three different regions: The metallic ring (temperature T_r), the slab of kapton (T_k) and the surrounding medium (T).

The metallic ring and the slab of kapton are considered as opaque materials and the radiant intensity in these regions is assumed null.

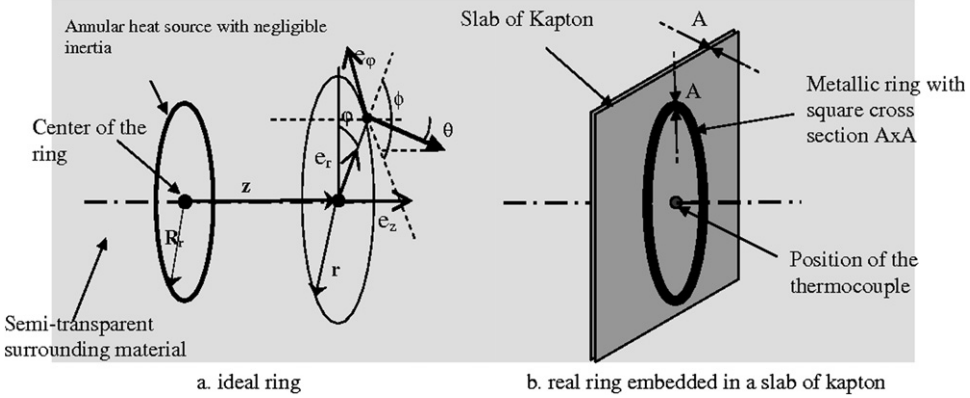

Fig. 1. Illustration of the cylindrical coordinate system around the ring.

2.2.1. Energy Equation in the surrounding material

The heat balance in a homogeneous semi-transparent, conductive but non-convective medium is governed by the energy equation which take into account the conductive and radiative heat transfer:

$$\rho C_p \frac{\partial T}{\partial t} = -\vec{\nabla}.\vec{q}_t = -\left(\vec{\nabla}.\vec{q}_c + \vec{\nabla}.\vec{q}_r\right) = k_c \frac{\partial^2 T}{\partial r^2} + \frac{1}{r} k_c \frac{\partial T}{\partial r} + k_c \frac{\partial^2 T}{\partial z^2} - \vec{\nabla}.\vec{q}_r \quad (2)$$

The phonic or effective conductivity of the material k_c depends on the temperature of the material. Nevertheless, for clarity purpose, we will omit to specify it afterwards.

2.2.2. Radiative Transfer Equation in the surrounding medium

Regarding the radiative heat transfer, the radiative flux is related to the intensity field in the medium:

$$\vec{q}_r = q_r^r \vec{e}_r + q_r^z \vec{e}_z \quad \text{with } q_r^r(r,z) = \int_{\Omega=4\pi} I(r,z,\theta,\varphi)\mu \, d\Omega$$

$$q_r^z(r,z) = \int_{\Omega=4\pi} I(r,z,\theta,\varphi)\xi \, d\Omega \quad (3)$$

and

$$\vec{\nabla}.\vec{q}_r = \frac{1}{r}\frac{\partial}{\partial r}\left(r q_r^r\right) + \frac{\partial q_r^z}{\partial z} \quad (4)$$

The radiation intensity field is governed by the Radiative Transfer Equation (RTE) described in details in [9]. For a 2-D axisymmetric radiative transfer in an homogeneous material with azimuthal symmetry, this equation is:

$$\frac{\mu}{r}\frac{\partial(rI(r,z,\theta,\varphi))}{\partial r} - \frac{1}{r}\frac{\partial(\eta I(r,z,\theta,\varphi))}{\partial \phi} + \xi \frac{\partial I(r,z,\theta,\varphi)}{\partial z} + \beta I(r,z,\theta,\varphi) = \kappa I^0(T) + \frac{\sigma}{4\pi}\int_{\Omega'=4\pi} P(\nu) I(r,z,\theta',\varphi') \, d\Omega' \quad (5)$$

We can notice that it is necessary to know the temperature field in the medium to solve the RTE and to determine the radiation intensity field.

2.2.3. Radiative boundary conditions

The boundary conditions at the interface between the surrounding medium and the ring or the slab of kapton are related to the emissivity of the kapton or ring:

$$I(r, A/2, \theta, \varphi) = \varepsilon_{k,r} I^0\left(T(r, A/2)\right) + \frac{1-\varepsilon_{k,r}}{\pi} \times \int_{\Omega'=2\pi;\ \xi'<0} I(r, A/2, \theta', \varphi').|\xi'| \, d\Omega' \quad \text{for } \xi > 0 \quad (6)$$

We also have the following relations for the radiative intensities far from the ring:

$$I(r \to \infty, z, \theta, \phi) = I^0(T_{\text{init}}) \quad \text{for } \mu < 0 \quad \text{and}$$
$$I(r, z \to +\infty, \theta, \phi) = I^0(T_{\text{init}}) \quad \text{for } \xi < 0 \quad (7)$$

2.2.4. Thermal boundary conditions

If we take into account the inertia of the ring, the radiative contribution and the presence of the kapton slab, the thermal boundary condition around the ring can be obtained from a heat balance:

$$\rho_r C_r V_r \frac{dT_r}{dt} = \dot{Q} - 2\pi\left(\left(R_r + \frac{A}{2}\right)^2 - \left(R_r - \frac{A}{2}\right)^2\right) \times \left(-k_c\left(\frac{dT}{dz}\right)_{z=\frac{A}{2}} + \left(q_r^z\right)_{z=\frac{A}{2}}\right) + 2\pi\left(R_r + \frac{A}{2}\right) A_r k_k \left(\frac{dT_k}{dr}\right)_{r=R_r+\frac{A}{2}} - 2\pi\left(R_r - \frac{A}{2}\right) A k_k \left(\frac{dT_k}{dr}\right)_{r=R_r+\frac{A}{2}} \quad (8)$$

where $V_r = \pi.((R_r + \frac{A}{2})^2 - (R_r - \frac{A}{2})^2)A$ is the volume of the metallic ring.

A similar relation is obtained if we apply a heat balance to a ring of kapton embedded in the kapton slab in contact with the surrounding material, except that no internal heat generation occurs.

The other boundary conditions are:

$$\text{For all } r \text{ and } z \text{ when } t \leqslant 0,\ T(r,z,t) = T_{\text{init}} \quad (9)$$

$$\text{For } r \to \infty \text{ or } z \to \infty,\ T(r,z,t) = T_{\text{init}} \quad (10)$$

3. Numerical resolution of the transient coupled heat transfer

In order to solve the energy equation (2) and to calculate numerically the variation of the temperature field in each region during the transient heat transfer, we use an explicit time marching technique. As it is necessary to know the temperature field to solve the RTE and to compute $\vec{\nabla}.\vec{q}_r$ in the surrounding material, an internal iterative process should be performed at each time step to produce consistency between the temperature profile and the radiation field. However, when the time interval between two time steps is small ($\Delta t < 0.1$ s in our study), this internal iterative process is superfluous and the temperature field at the new time step could be calculated directly using the radiation intensity field at the previous time step without causing errors. In their study on the temperature rise of a cylindrical glass gob, Viskanta and Lim [10] use the same simplification.

3.1. Resolution of the energy equation and computation of the temperature field

At each time step, the resolution of the energy equation permits to compute the new temperature distribution from the temperature and radiation intensity profiles at the previous time step. To solve this equation we use a spatial discretization dividing the surrounding material in $nR \times nZ$ elementary volume (see Fig. 2). As the plane $z = 0$ is a plane of symmetry, we only consider the heat transfer in the region $z > 0$. In order to limit the computation time and memory requirement, the heat transfer problem is solved in a finite volume around the ring. Then the

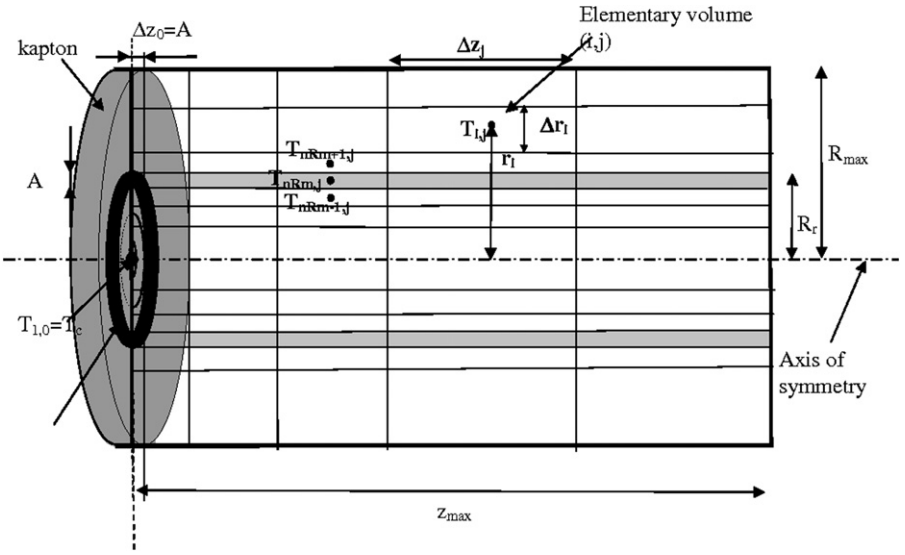

Fig. 2. Illustration of the spatial discretization around the ring.

calculations are restricted to $0 < r < R_{\max}$ and $0 < z < z_{\max}$. This volume must be sufficiently large to make sure that the theoretical temperature profile at the center of the ring is not influenced by the value of $R_{\max}$ and $z_{\max}$. A node is placed at the center of each elementary volume of coordinate r_i and z_j. The numerical resolution computes the evolution of the temperature (noted $T_{i,j}$) at this node.

According to the discretization used, the nodes $(i, 0)$, $i = 1, nR$, corresponds to the ring or the kapton slab. Moreover, the discretization along the z-axis provides narrower volumes near the ring where important temperature gradients are found. Then, we have:

$$\Delta z_0 = A$$
$$\Delta z_j = \left[\cos\left(\frac{(j-1)\pi}{2nZ}\right) - \cos\left(\frac{j\pi}{2nZ}\right)\right]\left(z_{\max} - \frac{A}{2}\right) \quad \text{for } j = 1, nZ \tag{11}$$

The discretization of the radius also provides narrower volumes near the ring. We distinguish three different regions for the discretization of the radius:

$$\text{for } i = 1, nRm-1;\ \{0 < r < R_r - A/2\}$$
$$\Delta R_{i+1} = \frac{\Delta R_i}{1.8} \quad \text{and} \quad \sum_{i=1}^{nRm-1} \Delta R_i = R_r - \frac{A}{2} \tag{12}$$
$$\Delta R_{nRm} = A \tag{13}$$
$$\text{for } i = nRm+1, nR;\ \{R_r + A/2 < r < R_{\max}\}$$
$$\Delta R_{i+1} = 1.8 \times \Delta R_i \quad \text{and}$$
$$\sum_{i=nRm+1}^{nR} \Delta R_i = R_{\max} - \left(R_r + \frac{A}{2}\right) \tag{14}$$

Then the radius r_{nRm} of the center of the nodes (nRm, j) corresponds to the radius R_r of the hot-ring and the temperature $T_{nRm,0}$ of the node noted $(nRm, 0)$ corresponds to its temperature.

For the nodes containing the semi-transparent surrounding medium, which are not in contact with the hot-ring or the kapton slab (nodes (i, j); $i = 1, nR$ and $j = 2, nZ$), if we express the energy equation (2) in a discretised form, we obtain:

$$T_{i,j}^{t+1} = T_{i,j}^{t} + \frac{\Delta t}{\rho C_p}\left[k_c \frac{\frac{T_{i+1,j}^t - T_{i,j}^t}{\Delta r_{i+1}/2 + \Delta r_i/2} - \frac{T_{i,j}^t - T_{i-1,j}^t}{\Delta r_i/2 + \Delta r_{i-1}/2}}{\Delta r_i} + \frac{k_c}{r_i}\frac{T_{i+1,j}^t - T_{i-1,j}^t}{\Delta r_i + \Delta r_{i-1}/2 + \Delta r_{i+1}/2} + k_c \frac{\frac{T_{i,j+1}^t - T_{i,j}^t}{\Delta z_{j+1}/2 + \Delta z_j/2} - \frac{T_{i,j}^t - T_{i,j-1}^t}{\Delta z_j/2 + \Delta z_{j-1}/2}}{\Delta z_j} - \left(\vec{\nabla}.\vec{q}_r\right)_{i,j}^t\right] \tag{15}$$

where $(\vec{\nabla}.\vec{q}_r)_{i,j}^t$ is the divergence of the radiative heat flux at the node i, j at time step t.

For the nodes of surrounding materials placed near the ring (nodes $(nRm, 1)$) or near the kapton slab (nodes $(i, 1)$; $i \neq nRm$) a similar discretised relation could be obtained by applying a energy balance.

The temperature of the ring nodes (nodes $nRm, 0$) and of kapton nodes (nodes $i, 0$ with $i \neq nRm$) at the new time step are obtained from the boundary conditions (Eq. (8)) expressed in a discretised forms.

Finally, the other thermal boundary conditions in a discretised form are:

$$T_{i,j}^0 = T_{\text{init}} \quad \text{for all } j \text{ and } i$$
$$T_{nR+1,j}^t = T_{\text{init}} \quad \text{for all } t \text{ and } j$$
$$T_{i,nZ+1}^t = T_{\text{init}} \quad \text{for all } t \text{ and } i \tag{16}$$

3.2. Resolution of the 2-D axisymmetric RTE using the discrete ordinates method

In order to calculate the radiative flux $(\vec{q}_r)_{i,j}$ and the radiative flux divergence $(\vec{\nabla}.\vec{q}_r)_{i,j}$ in each point of the spatial

discretization, it is necessary to solve the 2-D axisymmetric Radiative Transfer Equation (5). Several numerical methods can be used to solve the RTE (spherical harmonics method, the zone method of HOTTEL, the ray-tracing methods ...). In our study, we use the Discrete Ordinates Method based on a spatial discretization of the area around the wire and on an angular discretization of the space. The angular discretization allows replacing the angular integrals by finite summations over n_d discrete directions m (μ_m, η_m, ξ_m) with given weighting factors w_m. For convenience purpose, the spatial discretization is the same as the one used for the numerical resolution of the energy equation. The 2-D discrete ordinates solution for a radiatively participating medium in a cylindrical enclosure has been widely described, notably by Carlson and Lathrop [11] or Jendoubi et al. [12] and we will not detail it in this article.

Once the discretised intensity field in the semi-transparent medium around the wire has been determined, the radiative flux and radiative flux divergence are calculated using the discretised form of Eqs. (3) and (4):

$$\left(q_r^r\right)_{i,j} = \left[\sum_{m=1}^{nd} I_{i,j}^m \mu_m w_m\right] \quad \text{and}$$

$$\left(q_r^z\right)_{i,j} = \left[\sum_{m=1}^{nd} I_{i,j}^m \xi_m w_m\right] \tag{17}$$

$$\left(\vec{\nabla}.\vec{q}_r\right)_{i,j} = \frac{1}{r_i}\frac{r_{i+1/2}(q_r^r)_{i+1/2,j} - r_{i-1/2}(q_r^r)_{i-1/2,j}}{\Delta r_i} + \frac{(q_r^z)_{i,j+1/2} - (q_r^z)_{i,j-1/2}}{\Delta z} \tag{18}$$

3.3. Validation of the numerical method

The numerical resolution of the 2-D axisymmetric radiative problem has been tested by comparing the results of our model with various published results [12,13] for different media where only radiative transfer occurs and for different radiative boundary conditions. The accuracy of the numerical method is strongly dependent on the quadrature used for the angular discretization. We have tested different S_N quadratures. The results obtained when using the quadrature points and weights of the S_6 scheme prove to be quite satisfactory in all cases and we will use this quadrature in all the following numerical calculations.

Concerning the entire 2-D transient radiation/conduction coupling problem, few previous results has already been published [14,15]. We have compared the results of our numerical model with these studies and found a good agreement. However, the results presented in these papers concern theoretical problems with boundary conditions notably different from the ones encountered in our hot-ring simulation. Thus, it seems to us that it is more suitable to illustrate the validity of our numerical resolution by comparing with hot-ring results available for two ideal cases:

- Infinite purely conductive medium ($\beta \to \infty, k_c = 0.035\ \mathrm{W\,m^{-1}\,K^{-1}}$) surrounding a thin hot ring with small inertia ($\rho_r C_r V_r \to 0$) without any kapton slab.
- Infinite transparent medium ($\beta = 0; k_c = 0.035\ \mathrm{W\,m^{-1}\,K^{-1}}$) surrounding a thin hot-ring with small inertia ($\rho_r C_r V_r \to 0$) without any kapton slab.

Although these two ideal cases are limiting, they seem to us more appropriate to illustrate the validations of the model as the boundary conditions are close to the real problem.

The two ideal test cases correspond to the heating of a hot-ring without any kapton slab. Then, in order to model them using the simulation previously described without taking into account the presence of the kapton, the computations were carried out by setting $\rho_k C_k = \rho C_p$ and $k_k = k_c$ and by replacing the radiative boundary condition (6) by the following ones:

$$I(R_r - A/2, z, \theta, \phi) = \varepsilon_r . I^0\big(T(r,0)\big) + \frac{1-\varepsilon_r}{\pi}. \int_{\Omega=2\pi;\ \mu'>0} I(R_r - A/2, z, \theta', \phi').|\mu'|.d\Omega'$$

$$\text{for } \mu < 0 \text{ and } \{z < A/2\} \tag{19}$$

$$I(R_r + A/2, z, \theta, \phi) = \varepsilon_r . I^0\big(T(r,0)\big) + \frac{1-\varepsilon_r}{\pi}. \int_{\Omega=2\pi;\ \mu'<0} I(R_r + A/2, z, \theta', \phi').|\mu'|.d\Omega'$$

$$\text{for } \mu > 0 \text{ and } \{z < A/2\} \tag{20}$$

$$I(r, 0, \theta, \phi) = I(r, 0, \pi - \theta, \phi)$$

$$\text{for } \{r > R_r + A/2 \text{ or } r < R_r - A/2\} \tag{21}$$

The first test case could be solved analytically as it corresponds to the ideal case described in Section 2.1. The variation of the temperature at the center of the ring is then given by Eq. (1). We compared the results of the analytical formula with the temperature rise predicted by our numerical simulation. We made two different numerical calculations. The first one delivers an exact numerical solution by setting $\vec{q}_{r_{i,j}}^{\,t} = \vec{0}$ and $(\vec{\nabla}.\vec{q}_r)_{i,j} = 0$ for all $i, j > 0$ and t. For the second calculation, we fixed β to a very large value ($\beta = 10^6\ \mathrm{m^{-1}}$). The other parameter used for the numerical resolution are $\rho_r C_r = 41\,500\ \mathrm{J\,m^{-3}\,K^{-1}}$, $R_r = 0.01$ m, $A = 0.0001$ m, ($\rho_r C_r V_r = 0.2607\ \mathrm{J\,K^{-1}}$), $k_r = 20\ \mathrm{W\,m^{-1}\,K^{-1}}$, $\rho = 32\ \mathrm{kg\,m^{-3}}$, $C_p = 800\ \mathrm{J\,kg^{-1}\,K^{-1}}$, $\dot{Q} = 0.063$ W, $T_{\mathrm{init}} = 296$ K, $nRm = 8$, $nR = 22$ and $nZ = 33$. For both calculations, we set $R_{\max} = 0.2$ m, $z_{\max} = 0.1$ m. We have checked that these values of $R_{\max}$ and $z_{\max}$ are sufficiently important in order for the numerical results to remain independent of their values. The results obtained then correspond to those of an infinite medium surrounding a ring of radius $R_r = 0.01$ m and width $A = 0.0001$ m.

The comparison between analytical and numerical results show that the temperature rise computed by neglecting radiative heat flux divergence or by setting $\beta = 10^6\ \mathrm{m^{-1}}$ are both very close to the analytical solution as the relative differences are always lower than 1% when $t > 33$ s. We notice that the maximum differences between analytical and numerical results are found for the very low values of time t. This can be explained by the fact that the low thermal inertia of the ring which influences the heat transfer at the beginning of the heating, is neglected by

the analytical solution whereas the numerical solutions take it into account.

Regarding the second test case, it corresponds to the transparency limit $\beta = 0$. Under this assumption, the conductive and radiative contributions can be evaluated separately as the surrounding medium does not participate to the radiative transfer ($(\vec{\nabla}.\vec{q}_r)_{i,j} = 0$). There is a direct radiative exchange between the ring and the medium at $T = T_{\text{init}}$, and the radiative heat flux emitted by the ring only depends on its emissivity and its local temperature. It can be evaluated by the analytical relation:

$$q^z_{r_{nRm,1/2}} = \varepsilon_r \sigma_{\text{SB}} \left(T^4_{nRm,0} - T^4_{\text{init}}\right) \quad \text{and}$$
$$q^r_{r_{nRm\pm1/2,0}} = \varepsilon_r \sigma_{\text{SB}} \left(T^4_{nRm,0} - T^4_{\text{init}}\right) \tag{22}$$

The numerical results obtained by setting $(\vec{\nabla}.\vec{q}_r)^t_{i,j} = 0$ and using the previous boundary conditions equation (22) with $\varepsilon_r = 1$ in the purely conductive problem have been compared to those obtained by setting $\beta = 10^{-6}$ m^{-1} in the numerical resolution of the conduction–radiation coupling. The deviation between the two numerical methods is always lower than 0.001 in the time range 15–600 s. Thus, the numerical resolution of the radiative problem proves to give satisfactory results.

As a conclusion the calculations carried out for the two limiting cases show that, when using the spatial discretization $nRm = 8$, $nR = 22$, $nZ = 33$ and the S_6 angular quadrature, our numerical method accurately simulates the temperature rise near the hot ring.

3.4. Influence of a non-complete ring source

The method of prediction of the heat transfer described in the previous paragraphs has been developed assuming that the metallic ring source from which the heat is generated was a complete circle. In reality, the experimental apparatus is not made of a complete ring source given that a thermocouple has to be introduced at the center of the circle. An opening is then made on the ring which is actually a circular arc covering an angle ψ of approximately 300°. In order to determine whether this opening could have an influence on the temperature at the center of the ring, we have developed a numerical resolution of the heat transfer with non-axisymmetric thermal boundary conditions. To simplify the problem, we only modeled a purely conductive heat transfer. The energy equation has, now, to take into account the influence of azimuthal angle φ:

$$\rho C_p \frac{\partial T(r,z,\varphi,t)}{\partial t} = k_c \frac{\partial^2 T(r,z,\varphi,t)}{\partial r^2} + \frac{1}{r} k_c \frac{\partial T(r,z,\varphi,t)}{\partial r} + k_c \frac{\partial^2 T}{\partial z^2} + \frac{k_c}{r} \frac{\partial^2 T(r,z,\varphi,t)}{\partial \varphi^2} \tag{23}$$

To solve this equation numerically, we use a discretization of the azimuthal angle dividing the 2π radians in $n\varphi$ equal volumes covering an angle $\Delta\varphi = \frac{2\pi}{n\varphi}$.

We carried out calculations with the parameters presented in Section 3.3 ($k_c = 0.035$ W m^{-1} K^{-1}) using a discretization of the azimuthal angle dividing the 2π radians in $n\varphi = 24$ equal volumes. We made the calculations for rings with $\psi = 11\pi/6$ radians ($n\varphi_r = 22$), $\psi = 3\pi/2$ radians ($n\varphi_r = 18$) and $\psi = 5\pi/6$ radians ($n\varphi_r = 10$). The comparison with the results obtained for a complete ring source reveal that the temperature rise at the center of the ring is practically not affected by the non-complete source. When $\psi = 11\pi/6$, the relative difference with the results computed for a complete ring is always lower than 0.1% when $t > 10$ s. For open rings with smaller values of ψ, this difference increases but remains relatively low. For example for an open ring which cover less than half a circle $\psi = 5\pi/6$, the deviation is lower than 1% when $t > 40$ s.

These observations could be explained by the fact that all the heat point sources constituting the hot-ring are equidistant from the center of the circle even when the ring is not complete. As a consequence, the formula (1) is still valid. The small differences observed for open rings may be due to the fact that the temperature field in the medium is no more axisymmetric and can slightly affect the temperature at the center.

However, as it was previously mentioned, all the hot-ring apparatus used experimentally in this study cover an angle ψ close to 300° ($5\pi/3$). We will then assume afterwards that the temperature at the center of these apparatus is not affected and all the corresponding computations will be carried out assuming a complete hot-ring.

4. Results and discussions

As explained in the introduction, the main purpose of the study is to determine whether the classical hot-ring method (based on a pure conduction solution) could be used for evaluating the equivalent thermal conductivity of low-density thermal insulators where both conductive and radiative heat transfer occur. To do that, we made a series of measurements of the temperature rise on four low-density EPS foams using different hot ring measuring systems and compared the results to numerical predictions. From these results, we could evaluate the theoretical or experimental thermal conductivity of the material estimated from the hot-ring method by identifying the conductivity k_{hot} which permits to best fit the experimental or the numerical temperature rise using Eq. (1). In practice this conductivity is identified at each time t by varying the value of k_{hot} until we have:

$$\frac{\dot{Q}}{4\pi k_{\text{hot}} R_r} \left[\operatorname{erfc}\left(\frac{R_r \cdot \sqrt{\rho C_p}}{\sqrt{(4k_{\text{hot}}(t+\Delta t)}} \right) - \operatorname{erfc}\left(\frac{R_r \sqrt{\rho C_p}}{\sqrt{(4k_{\text{hot}}(t-\Delta t)}} \right) \right] = T_{\text{exp./num.}}(t+\Delta t) - T_{\text{exp./num.}}(t-\Delta t) \tag{24}$$

where $T_{\text{exp./num.}}(t)$ is the experimental or numerical temperature at time t at the center of the ring

For the experimental results, in order to limit the fluctuations, the value of Δt used for the identification is $\Delta t = 15$ s, whereas, for numerical results, we used $\Delta t = 1$ s.

An analysis of the influence of the different parameters has also been conducted.

4.1. Description of the low-density thermal insulators used

Measurements have been made on four different EPS foams in which radiative heat transfer has been proved to play a significant part of the total heat transfer. The foams used have been characterized in a previous study dealing with the modeling of heat transfer in low-density EPS foams [7]. Their equivalent thermal conductivities $k_{\text{eq.m}}$ have been measured by the guarded hot-plate method for an average temperature of 296 K. These equivalent conductivities can be taken as references. The global radiative properties of the foams (β, ω and $P(\nu)$) needed for the numerical simulation have been determined theoretically in the previous study [7] from their measured structural characteristics such as density or mean cell diameter. The validity of the model used has been checked by comparing experimental transmittance and reflectance measurements on thin slab of foams with the calculated ones obtained using the theoretical monochromatic radiative properties. Moreover, their conductive property (k_c) has also been determined from validated theoretical model of the literature. Thus, we could compute the theoretical equivalent thermal conductivity $k_{\text{eq.th}}$ from the radiative and conductive properties by solving numerically the steady-state one-dimensional coupled heat transfer using the discrete ordinates method in Cartesian coordinates and the control volume method. Given that the radiative contribution is relatively important in the EPS foams studied, their theoretical equivalent conductivity varies with the boundary conditions and especially with the average temperature of the material. For the temperature range 296–320 K, the variation of $k_{\text{eq.th}}$ for the four EPS foams have proved to follow the law:

$$k_{\text{eq.th}} = aT^2 + bT + c \tag{25}$$

where a (W m^{-1} K^{-3}), b (W m^{-1} K^{-2}) and c (W m^{-1} K^{-1}) are constants peculiar to each foam.

All the characteristics of the four EPS foams are regrouped in Table 1 except the heat capacity, which is given for each foam sample by the relation:

$$C_p = \frac{(\rho - \rho_{\text{air}})C_{PS} + \rho_{\text{air}}C_{\text{air}}}{\rho} \quad \text{with } C_{\text{air}} = 1006\ \text{J kg}^{-1}\,\text{K}^{-1}$$
$$\text{and} \quad C_{PS} = 1200\ \text{J kg}^{-1}\,\text{K}^{-1} \tag{26}$$

Regarding the sample number 4, we checked that it is sufficiently dense to be considered as an optically thick medium contrary to the other lighter samples. For this sample, the radiative heat transfer problem is then treated using the Rosseland approximation. This approximation allows to relate directly the radiative flux to the temperature gradient and greatly simplifies the resolution:

$$q_r^r = -\frac{16\sigma_{\text{SB}}}{3\beta_{\text{ROSS}}}T^3\frac{\partial T}{\partial r}; \qquad q_r^z = -\frac{16\sigma_{\text{SB}}}{3\beta_{\text{ROSS}}}T^3\frac{\partial T}{\partial z} \tag{27}$$

4.2. Description of the hot-ring apparatus

The hot-ring measuring system used is composed of different apparatus (see Fig. 3):

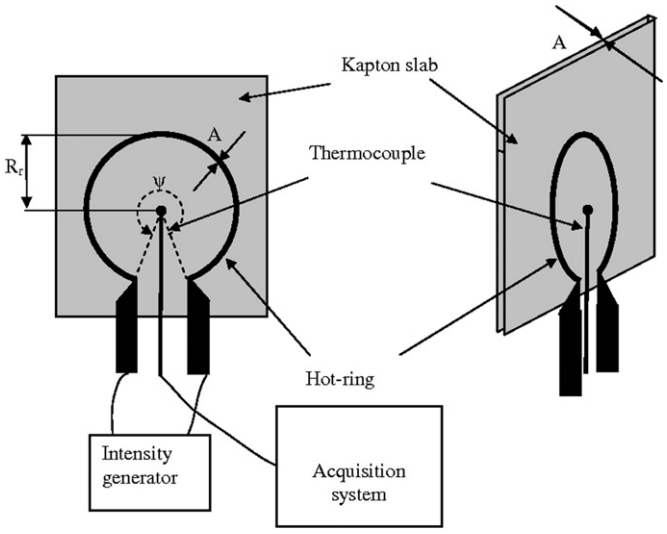

Fig. 3. Illustration of the structure of the hot-ring apparatus.

- The measuring apparatus including the heated ring and a thermocouple placed at the center of the ring.
- A current generator supplying the hot-ring.
- An acquisition system connected to the thermocouple allowing to record the temperature rise with a time step of 1 s.

As it was previously explained, in order to ensure that the thermocouple and the ring are well positioned, the two elements are embedded in a slab of kapton of the same thickness as the metallic ring (see Fig. 3).

The characteristics of the hot-ring apparatus used are: radius $R_r = 0.01$ m and thickness $A = 180$ μm. The hot-ring is made of a constantan track whose thermal properties are: $\rho_r = 8900$ kg m^{-3}, $C_r = 415$ J kg^{-1} K^{-1} and $k_r = 10$ W m^{-1} K^{-1}. The thermal properties of the kapton slab are: $\rho_k = 1420$ kg m^{-3}, $C_k = 1090$ J kg^{-1} K^{-1} and $k_k = 0.2$ W m^{-1} K^{-1}.

Concerning the emissivity of the ring and of the kapton slab, it is difficult to determine them precisely. However, in order to estimate it, we made transmittance and reflectance measurements on thin slabs (≈200 μm thick) of kapton and reflectance measurements on sheets of constantan using an FTIR spectrometer. The experimental results show that a slab of kapton of 200 μm thick could be considered as opaque and purely absorbing and that the constantan has a very low reflectivity in the Medium Infrared Radiation range (2 μm $< \lambda <$ 25 μm). As a consequence, we will assume that the metallic ring and the kapton slab are perfectly emissive: $\varepsilon_r = \varepsilon_k = 1$.

The intensity generator permits to supply the ring of constantan with electric current and to dissipate a certain heat rate $\dot{Q}$ by Joule effect. The heat generated is proportional to the square of the current provided and to the electrical resistance Ω_r of the ring. This resistance has been measured using a multimeter and is 6 Ω for the hot-ring used.

Table 1
Thermal characteristics of the four low-density EPS foams used

Sample number	ρ (kg m^{-3})	$k_{eq.m}$ (W m^{-1} K^{-1}) at 296 K	β (m^{-1})	ω	g	a (W m^{-1} K^{-3}), b (W m^{-1} K^{-2}), c (W m^{-1} K^{-1})	$k_{eq.th}$ (W m^{-1} K^{-1}) at 296 K
1	10	0.0482	608.2	0.905	0.58	$a = 8.878 \times 10^{-7}$; $b = -2.09 \times 10^{-4}$; $c = 0.0344$	0.05003
2	12.6	0.0428	763.9	0.901	0.58	$a = 7.606 \times 10^{-7}$; $b = -1.808 \times 10^{-4}$; $c = 0.0328$;	0.04554
3	18.3	0.0396	1072.4	0.889	0.6	$a = 5.308 \times 10^{-7}$; $b = -9.081 \times 10^{-5}$; $c = 0.02189$	0.04136
4	32.0	0.03395	$\beta_{ROSS} = 1400$	–	–	$a = 2.636 \times 10^{-7}$; $b = -2.46 \times 10^{-5}$; $c = 0.01803$	0.03395

4.3. Comparison of experimental and numerical results

We have used the hot-ring apparatus previously and measured the temperature rise at the center of the ring for each of the EPS foam samples presented. We made temperature rise measurements for the time range 1–600 s with different heating power $\dot{Q}$. The measurements are made by placing the hot-ring apparatus embedded in the slab of kapton between two slabs of the foam sample considered. In order to ensure a good thermal contact between the hot-ring and the sample, the two slabs are slightly compressed using a heavy object. The dimensions of the foam slabs used are sufficiently important to consider that the porous medium surrounding the heated-wire is infinite.

We also carried out the corresponding numerical calculation for each EPS foams samples using the conductive and radiative properties and the densities illustrated in Table 1 and the properties of the ring presented in Section 4.2. In each case, the initial temperature of the materials is: $T_{init} = 296$ K.

The thermal contact resistance between the ring and the slab of kapton and the surrounding medium is neglected.

The numerical parameters used are: $nRm = 8$; $nR = 22$; $nZ = 33$; S_6 quadrature; $z_{max} = 0.1$ m and $R_{max} = 0.2$ m. The values of R_{max} and z_{max} have been chosen in order for the numerical results to remain independent of their values.

4.3.1. Influence of the kapton slab

We have seen that the presence of the slab of kapton on classical hot-ring apparatus could disturb the propagation of the heat around the hot-ring. In order to evaluate the influence of this slab, we made measurements on sample N° 4 using the hot-ring apparatus N° 4 before and after having partially removed the kapton slab. This has been done by cutting the kapton with a scalpel. We obtained three different configurations for the kapton slab, which are illustrated on Fig. 4. The thickness B of the kapton still present around the hot-ring for the third configuration illustrated on Fig. 4 is approximately 1 mm and the radius R_{th} of the kapton present around the thermocouple is approximately 500 μm. Then the three configurations could be described by:

- Configuration 1: kapton slab present for all r.
- Configuration 2: kapton slab present for $r < R_r + B/2$.
- Configuration 3: kapton slab present for $r < R_{th}$ and $R_r - B/2 > r > R_r + B/2$.

At the same time, we also carried out the simulations of temperature rise at the center of the ring for foam sample N° 4 and for fictitious hot-ring apparatus corresponding to the three different configurations of the kapton slab. This has been done by replacing the density ρ_k, the heat capacity C_k and the thermal conductivity k_k of the kapton by the corresponding properties (ρ, C_p and k_c) of the EPS foam for the nodes which are no more occupied by the kapton slab (nodes $(i, 0)$ with $r_i > R_r + B/2$ for configuration 2 and nodes $(i, 0)$ with $r_i > R_r + B/2$ or $R_{th} < r_i < R_r - B/2$ for configuration 3). The comparison between the temperature rises obtained experimentally and numerically for the three configurations is illustrated on Fig. 5 for a heating power $\dot{Q} = 0.135$ W. We also show the theoretical

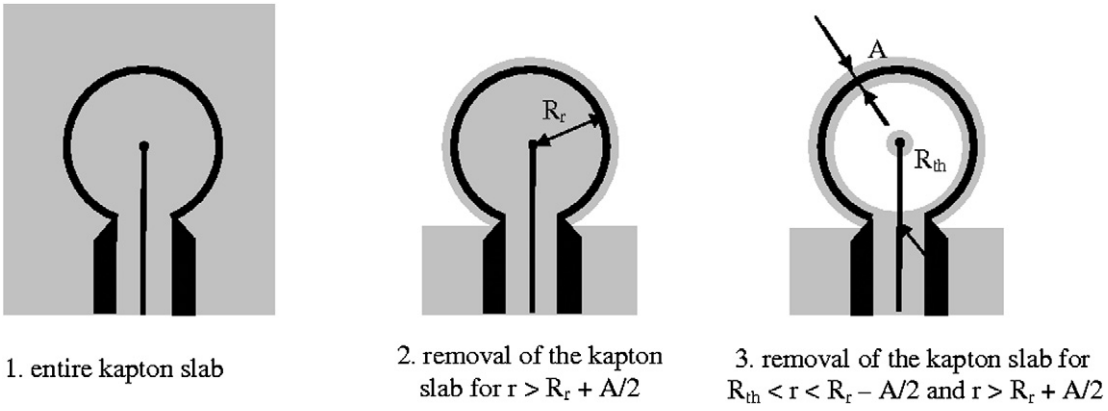

Fig. 4. Illustration of the three different configurations of the hot-ring apparatus N° 1 after the removal of the kapton slab.

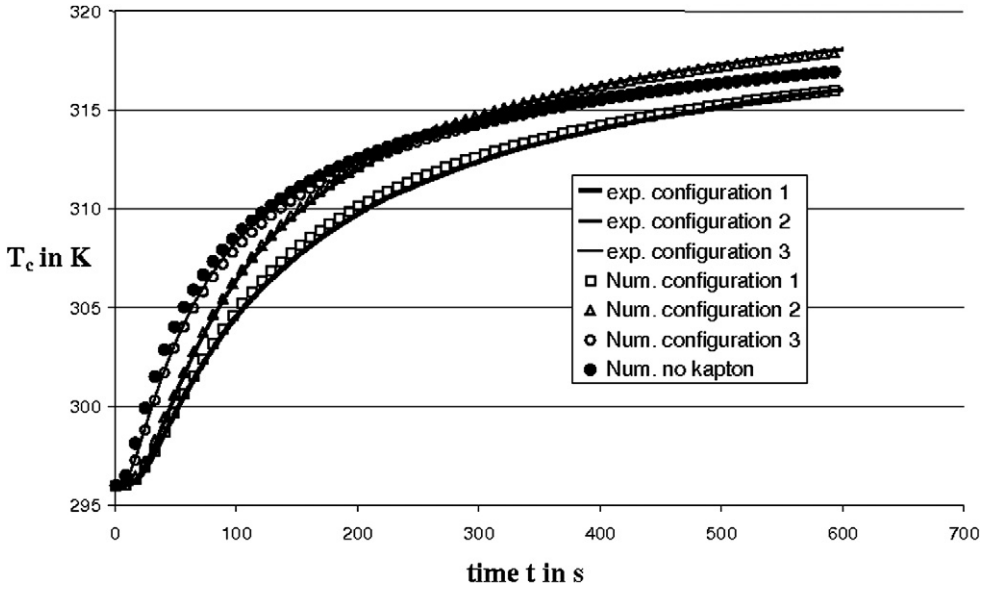

Fig. 5. Comparison between experimental and numerical evolution of the temperature for the three different configuration of the hot-ring apparatus.

evolution of T_c in the ideal case where there was no kapton slab at all. The parameters used for the computation are the same as those of Section 3.3.

The results depicted on Fig. 5 show that the presence of kapton has a strong influence on the temperature rise at the center of the hot-ring apparatus. Indeed, the numerical and experimental temperature rise obtained in the different configurations are in good agreement and reveal that the slab of kapton tends to slow down the heat transfer from the hot-ring to the center of the circle. This can be explained by the fact that the thermal inertia of kapton slab ($\rho_k C_k = 1.55 \times 10^6$ J m^{-3} K^{-1}) is much more important than that of the surrounding medium with low density ($\rho C_p = 38\,400$ J m^{-3} K^{-1}). As a consequence, a more important amount of heat and then a more important heating duration is required to reach the same temperature level when a piece of kapton is present. The heat transfer is then strongly affected when the hot-ring measuring method is applied to low-density materials such as EPS foams. Fig. 5 also shows that when the kapton only occupies the area $r < R_r + B/2$, the temperature T_c reaches larger values than when the kapton slab is complete. As it was expected, we could also notice that in configuration 3 (only a thin width of kapton present around the ring), the evolution of the temperature is very close to the ideal case where no kapton is present at all.

In order to determine whether Eq. (1) still describes the evolution of the temperature T_c when kapton is present, we have computed the temperature rise T_c for a purely conductive medium with $k_c = 0.035$ W m^{-1} K^{-1} and $\rho C_p = 38\,400$ J m^{-3} K^{-1} in the three different configurations and identified the evolution of the conductivity k_{hot} estimated from the numerical temperature rise (Eq. (24)). The results are illustrated on Fig. 6 and are referenced as classical identification (classic. ident.). The figure shows that when no kapton is present (ideal case), the identification procedure permits to estimate very accurately the thermal conductivity k_c of the surrounding material as soon as t is greater than approximately 50 s. However when a piece of kapton is present (configuration 1 or 3), Eq. (1) no more describes faithfully the evolution of the temperature at the center of the apparatus. The value of k_{hot} identified varies with the time t and does not correspond to k_c. The error in the estimation of k_c is not negligible and higher when a more important quantity of kapton is present. Thus, the classical hot-ring measuring method is not adapted for the measurement of the thermal conductivity of low-density thermal insulators.

To overcome the problem due to the presence of the kapton slab, which disturbs the heat transfer, we have developed a modification of the identification procedure, which takes into account the delay of the temperature rise when kapton is present. This modification is based on the numerical predictions computed with and without the kapton slab. The principle is to modify the measurement time t into time t_{mod} corresponding to the time, which would be required from the beginning of the heating to reach the same value of T_c in the case where no kapton was present. Then, the use of the modified time t_{mod} instead of the real measurement time t in the identification procedure described in Section 4 permits to estimate the effective (phonic) thermal conductivity k_c of the material with a good accuracy. The relation between t_{mod} and t could be determined from the numerical predictions of temperature rise with and without the kapton slab by computing, for each measurement time t, the corresponding value of t_{mod}, which leads to the same elevation of temperature ΔT_c. We have shown that, in the case of a hot-ring apparatus with a kapton slab used on a low density thermal insulators, the evolution of t_{mod} with t could be fitted very accurately using a relation of the form:

$$t_{\text{mod}} = a_6 t^6 + a_5 t^5 + a_4 t^4 + a_3 t^3 + a_2 t^2 + a_1 t + a_0 \tag{28}$$

The values of the parameters a_i (units: s^{-i+1}) depend on the properties of the kapton slab and hot-ring (R_r, ρ_k, C_k, k_k, A, ρ_r, C_r and k_r) but also on the thermal properties of the surrounding material in which the measurement is made. For example, when measurement is made on a purely conductive thermal

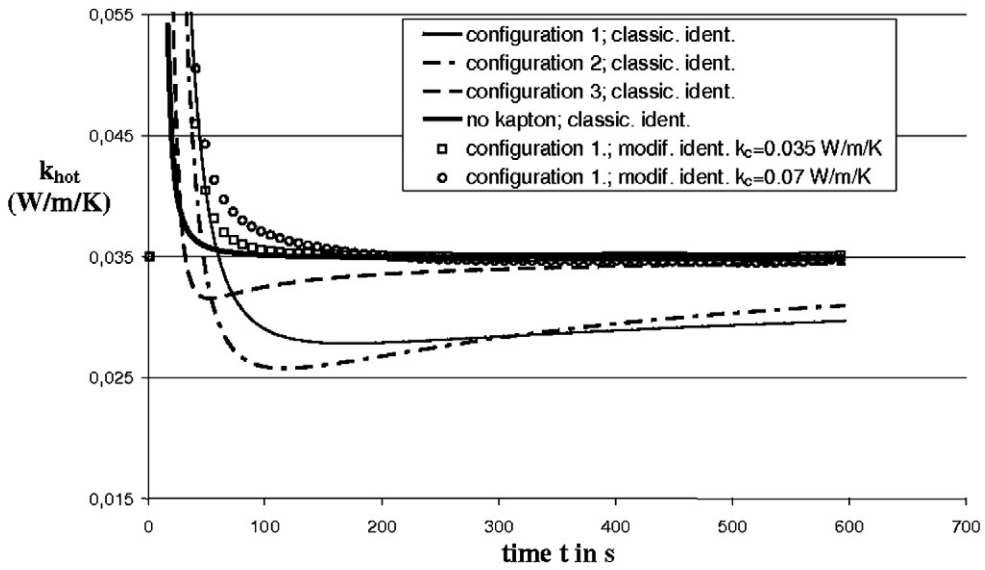

Fig. 6. Evolution of the conductivity k_{hot} estimated from the numerical temperature rise in different configurations using the classical identification procedure (classic. ident.) and the modified identification procedure (modif. ident.).

insulator with the properties $\rho C_p = 38\,400\ \text{J kg}^{-1}\,\text{K}^{-1}$ and $k_c = 0.035\ \text{W m}^{-1}\,\text{K}^{-1}$ using hot-ring apparatus N° 1 ($R_r = 0.01$ m, $\rho_k C_k = 1.55 \times 10^6\ \text{J m}^{-3}\,\text{K}^{-1}$, $k_k = 0.2\ \text{W m}^{-1}\,\text{K}^{-1}$, $A = 180$ μm, $\rho_r = 8900\ \text{kg m}^{-3}$, $C_r = 415\ \text{J kg}^{-1}\,\text{K}^{-1}$ and $k_r = 10\ \text{W m}^{-1}\,\text{K}^{-1}$) with complete kapton slab, we have:

$$t_{\text{mod}} = 5.63 \times 10^{-15} t^6 + 1.28 \times 10^{-11} t^5 + 1.21 \times 10^{-8} t^4 + 6.17 \times 10^{-6} t^3 + 1.96 \times 10^{-3} t^2 + 0.417 t + 0.184 \quad (29)$$

The evolution of the thermal conductivity k_{hot} estimated from the temperature rise in the presence of a complete kapton slab (configuration 1) using this modified identification procedure is depicted on Fig. 6 (modif. ident.). One can see that the new identification procedure estimates very accurately the conductivity of the surrounding material after a time t of approximately 100 s, and thus it permits to eliminate the perturbations of the heat transfer due to the kapton slab. The main problem of the modified identification procedure is that, in order to determine the parameter a_i of Eq. (29), one has to know, a priori, the value of the thermal conductivity k_c, which precisely has to be measured. However, in practice, given that the delay of the temperature rise due to the kapton slab is especially due to the inertia effects, the thermal conductivity of the surrounding material has only a very slight influence on Eq. (29). Thus, it is sufficient to simply know the order of magnitude of k_c to determine a relation, which is accurate enough. To illustrate this, we have depicted on Fig. 6 the evolution of the conductivity k_{hot} estimated from the numerical temperature rise of configuration 1 (complete kapton slab) using the modified identification procedure with a value, a priori, of $k_c = 0.07\ \text{W m}^{-1}\,\text{K}^{-1}$. One can remark that even when the value of k_c used for the estimation of Eq. (29) is notably different (two times greater) from the real thermal conductivity, the modified identification procedure allows to determine an accurate value of k_{hot}. The time necessary for k_{hot} to converge to the exact value of k_c is a little more important than when the right conductivity is used but remain relatively low (approximately 150 s in our case). Our modified identification procedure could then be used with a good accuracy if the order of magnitude of k_c is known and thus, the hot-ring measuring method using classical hot-ring apparatus could be extended to low-density materials, which are purely conductive.

4.3.2. *Influence of the foam sample: Radiation effects*

In the previous paragraph, we have shown that the classical hot-ring method is not adapted to the measurement of the thermal conductivity of low-density conductive materials given that the presence of the slab of kapton disturbs the heat transfer. The results of the classical hot-ring method then lead to noticeable errors for this kind of medium. Therefore, we developed a new procedure allowing to eliminate the influence of the inertia of the slab during the identification of the conductivity k_{hot} and to extend theoretically the method to the low-inertia conductive materials.

However, in most of the real low-density materials such a low-density thermal insulators, the solid matrix is no not sufficiently dense to consider that the material is opaque to the infrared thermal radiation. The materials are said to be semi-transparent and a significant part of the total heat flux is transferred by radiation. Thus, another problem appears if we would like to apply the hot-ring method to real low-density materials. Indeed, Eq. (1) is only valid for purely conductive materials. As a consequence, the hot-ring measuring method could theoretically not be used on low-density materials where the radiative contribution is not negligible. To analyze the influence of the radiative contribution and determine whether the hot-ring method could be extended to materials where radiative heat transfer occurs, we have compared the experimental and numerical results obtained for the four EPS foam samples presented in Section 4.1. These foams behave like semi-transparent materials for which the radiative contribution is more or less significant

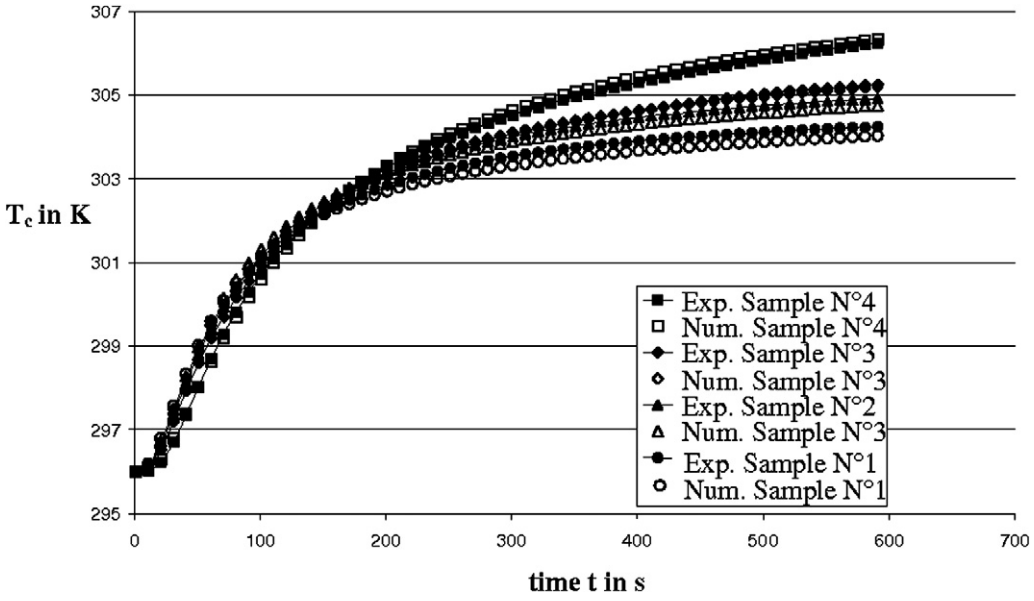

Fig. 7. Comparison of the temperature rise obtained experimentally and numerically for the four EPS sample using a heating power $\dot{Q} = 0.063$ W.

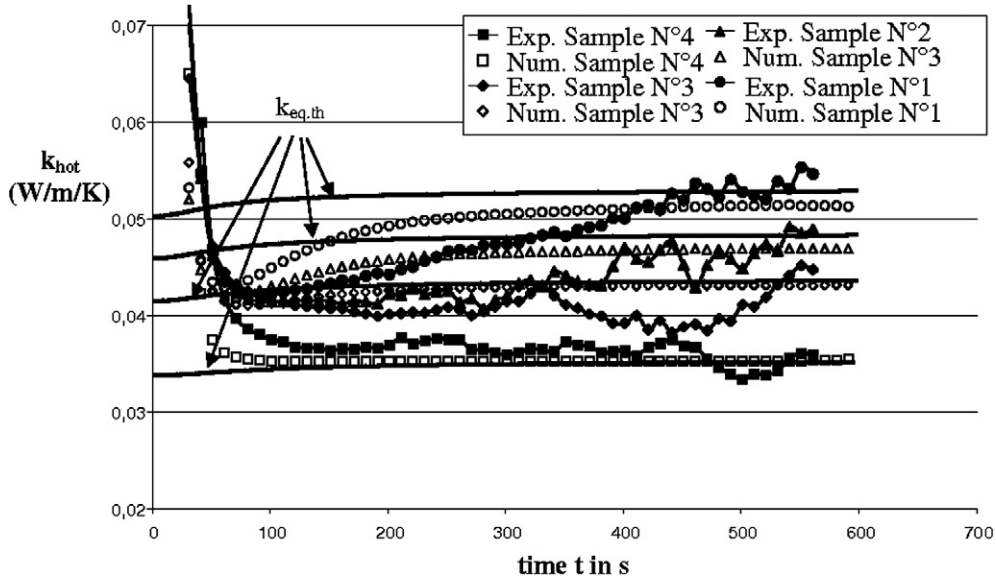

Fig. 8. Comparison of the estimated thermal conductivity k_{hot} obtained from the experimental and numerical temperature rise using the modified identification procedure for the four EPS sample.

(see Section 4.1). The comparison of experimental and numerical temperature rises for a heating power $\dot{Q} = 0.063$ W using the hot-ring described in Section 4.2 is illustrated on Fig. 7. The results have been obtained by using or simulating the classical hot-ring apparatus with a complete kapton slab. From these numerical and experimental temperature rises, we also have identified, for each EPS foam sample, the corresponding thermal conductivity using the modified identification procedure described in Section 4.3.1 which permits to eliminate the influence of the kapton slab. The whole results are regrouped on Fig. 8 where we also have depicted the evolution of the theoretical equivalent conductivity $k_{eq.th}$ for each foam.

One can notice that the accordance between the numerical and experimental evolutions of the temperature at the center of the ring is very good for each of the foam sample studied. We observe that the temperature level reached at the end of the measurement is more important for the denser foams.

With regards to the evolution of the estimated conductivity k_{hot}, the accordance between numerical and experimental results is not as remarkable as for the temperature rise but remains relatively good, especially, the classification of the foam according to their thermal conductivity is well-predicted by the experimental results. The fluctuations observed for the experimental results are due to the discrete evolution of the temperature measured by the thermocouple. If we compute the average relative difference between numerical and experimental k_{hot} in the time range 150–600 s we obtain 3.8% for sample N° 4, 5.6% for sample N° 3, 5.8% for sample N° 2 and 5.3% for samples

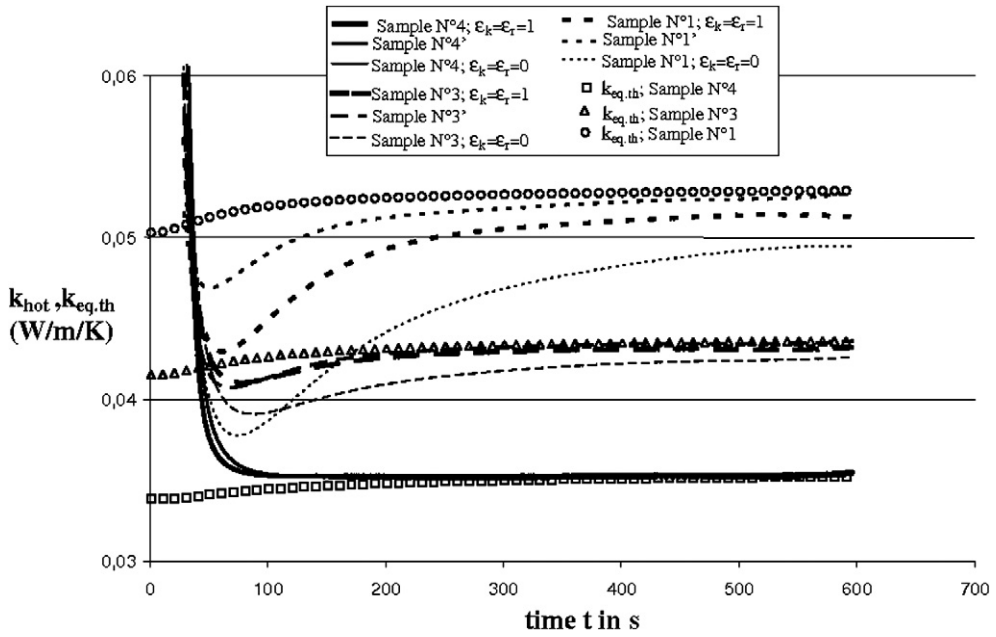

Fig. 9. Comparison of the numerical k_{hot} of samples N° 1, 3 and 4 calculated for a perfectly emissive ($\varepsilon_k = \varepsilon_r = 1$) or a perfectly non emissive ($\varepsilon_k = \varepsilon_r = 0$) apparatus or assuming purely conductive foam samples (samples N° $1'$, $3'$ and $4'$).

N° 1. We can remark that the evolutions of k_{hot} estimated from numerical temperature rises converge to the theoretical equivalent thermal conductivity $k_{\text{eq.th}}$ for samples N° 4 and 3, but reaches slightly lower values for samples N° 2 and 1 even for very important measurement time ($t \to 600$ s). These differences may be due to the importance of radiative contribution in these extremely light foam samples. One can also remark that the convergence of the numerical k_{hot} to the equivalent thermal conductivity $k_{\text{eq.th}}$ is faster for dense foam sample.

In order to characterize more precisely the contribution of the radiative heat transfer to the evolution of the estimated k_{hot}, we conducted additional simulations. Then, we considered four fictitious sample noted N° $1'$, $2'$, $3'$ and $4'$ having the same physical characteristics (ρ, C_p) and the same equivalent conductivity $k_{\text{eq.th}}$ as samples N° 1, 2, 3 and 4 but, in which, the heat transfer is assumed purely conductive ($k_c = k_{\text{eq.th}}$; $\beta \to \infty$). We also conducted simulations for the four EPS foams in the fictive case where the emissivities of the ring and of the kapton slab were null (perfectly reflective slab). The comparison between the evolution of k_{hot} for the fictitious materials ($1'$, $2'$, $3'$ and $4'$) and for the real EPS as well as the analysis of the numerical differences observed when the emissivity of the slab goes from 1 to 0 would give us more indications on the influence of the radiative contribution. The entire results (real sample, fictitious sample and $\varepsilon_k = \varepsilon_r = 0$) are illustrated on Fig. 9 where we also have depicted the evolution of the theoretical equivalent conductivity $k_{\text{eq.th}}$. For clarity purpose we have not represented the evolution of the different k_{hot} and $k_{\text{eq.th}}$ for samples N° 2 and $2'$.

The analysis of the results leads to several remarks:

First, the results obtained with the fictitious purely conductive materials (N° $1'$, $3'$ and $4'$) indicate that after a certain time t the identified k_{hot} converges to the equivalent conductivity $k_{\text{eq.th}}$ of the materials. Therefore, our modified identification procedure permits to determine an accurate value of the conductivity of the material. The time t required for k_{hot} to converge to the equivalent conductivity varies only slightly with the medium considered and is approximately 80 to 100 s if a relative accuracy of 5% is required.

Secondly, one can remark that when the model takes into account the radiative contribution and the real apparatus (samples N° 1, 3 and 4 with $\varepsilon_k = 1$), k_{hot} does not fit exactly the evolution obtained for the corresponding purely conductive materials. For samples N° $4'$ and 4, which is optically thick, the relative difference is practically imperceptible and the estimated conductivity calculated for sample 4 converges exactly to the equivalent conductivity. On the other hand, for samples N° 3 and especially N° 1, which are not optically thick materials, the value of k_{hot} does not converge exactly to $k_{\text{eq.th}}$ but reaches a slightly lower value. These convergence values are respectively 1% and 3% lower than $k_{\text{eq.th}}$ for samples N° 3 and 1. One can notice that these differences are almost negligible. Fig. 9 also shows that for the real foams, the convergence of k_{hot} is slower than for the corresponding fictitious purely conductive medium. For example, the time required to reach a value of k_{hot} which is 5% different from that obtained at $t = 600$ s is 90 s for sample N° 3 and 180 s for sample N° 1. Then, the lighter the foam is, the slower k_{hot} converges.

Finally, substantial differences are found between the numerical results obtained assuming non-emissive or perfectly emissive apparatus except for sample N° 4. For the other foam samples, the estimated conductivity k_{hot} computed with a non-emissive apparatus ($\varepsilon_k = \varepsilon_r = 0$) converge to slightly lower values than when $\varepsilon_k = \varepsilon_r = 1$. The relative difference after a measurement time $t = 600$ s are 1.4% and 3.6% for samples N° 3 and 1 respectively. These observations could be easily explained by the fact that when the emissivities ε_k and ε_r of the apparatus get lower, the radiative energy emitted and thus trans-

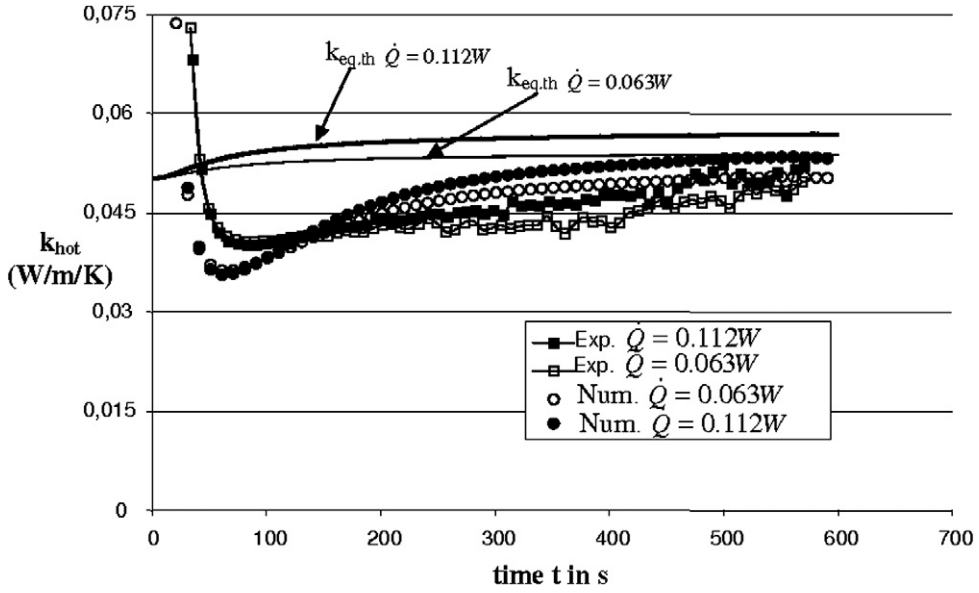

Fig. 10. Evolution of the numerical and experimental conductivity k_{hot} for sample N° 1 and different heating powers.

ferred in the material is less important and all is going on as if the equivalent conductivity of the material was lower. On the other hand, the emissivity of the apparatus does not influence the estimated conductivity for sample N° 4. Indeed, in this optically thick material, the mean free path of photons is much lower than the dimensions of the material and thus, the radiant intensity field and the radiative heat flux inside the medium are not affected by the intensity emitted by the apparatus.

As a conclusion, the comparison of the numerical results in the different fictitious cases show that, when the materials considered behaves like optically thick media, the hot-ring measuring method with the modified identification procedure permits theoretically to determine exactly the equivalent thermal conductivity of the materials although the heat transfer is not purely conductive. Moreover, this value is not affected by the emissivity of the apparatus. On the other hand, when the density of the semi-transparent materials is not sufficient for the Rosseland approximation (Eq. (27)) to be valid, the thermal conductivity identified after a sufficient measurement time is not consistent with the equivalent thermal conductivity measured by the guarded hot plate method. The more transparent the foam is, the more important the error is. Moreover this error depends on the emissivity of the apparatus used, and a perfectly emissive apparatus is theoretically required to minimize it. However, we have seen that the classical hot-ring apparatus could be considered as perfect emitter. Moreover, the maximum difference observed numerically when $\varepsilon_k = \varepsilon_r = 1$ for sample N° 1 which constitutes the lighter EPS foam obtainable is approximately 3%. This value is lower than the measurement uncertainty of most of the guarded hot plate apparatus and is almost negligible. Thus, it seems to us that the hot-ring method using classical apparatus and the modified identification procedure could be extended to all materials, even the very light insulators, with an acceptable accuracy.

4.3.3. *Influence of the heating power* $\dot{Q}$

In order to confirm the accordance between numerical and experimental results, we have studied the influence of the heating power $\dot{Q}$ in both cases by measuring and simulating the temperature rise for $\dot{Q} = 0.063$ W and $\dot{Q} = 0.112$ W using a hot-ring apparatus different from that presented in Section 4.2 with the following characteristics: $R_r = 0.0075$ m; $A = 230$ μm, $\Omega_r = 2.8$ Ω and $\varepsilon_r = \varepsilon_k = 1$. We present the results obtained for the sample N° 1 on Fig. 10 where we also depict the evolution of $k_{\text{eq.th}}$ for the two heating powers.

As it can be observed, the heating power has a slight but non-negligible influence on the thermal conductivity measured. Indeed, both experimental and numerical results show that a high heating power leads to a higher value of the conductivity measured. This is not surprising given that the equivalent thermal conductivity of the EPS foams increases with the temperature (Eq. (24)). This is especially due to the fact that radiative heat transfer, which is significant in foam sample N° 1, is strongly dependent on the temperature. The accordance between the estimated conductivity obtained experimentally and numerically using the modified identification is still very good. As it has been noticed in the previous paragraph, one can remark that owing to the importance of radiative heat transfer, the conductivity k_{hot} identified from the numerical results does not converge exactly to the equivalent thermal conductivity $k_{\text{eq.th}}$. The relative difference is almost independent of the heating power supplied. As a conclusion, one should always refer to the heating power used when measuring the thermal conductivity with the hot-ring method.

5. Conclusions

The hot-ring method is a transient technique for measuring the thermal conductivity of materials whose principle is very close to he widely known hot-wire method. It could present an interest for measurements on low-density thermal insula-

tors for which the hot-wire method has been proved to be poorly adapted. Indeed, for these materials, due to the limited length of classical hot-wire apparatus, the assumption of one-dimensional heat transfer is not valid during all the measurement duration. On the other hand, the hot-ring technique does not make any assumption on the dimension of the heating elements. In this paper, we investigated numerically and experimentally the use of this technique for the measurement of the equivalent thermal conductivity of low-density EPS foams in which both conductive and radiative heat transfer occur.

First, we observed that the numerical and experimental results are in good agreement and then that our numerical model simulates satisfactorily the measuring technique. Numerical and experimental investigations also revealed that, owing to the presence of a slab of kapton ensuring the positioning of the thermocouple, the thermal inertia of classical hot-ring apparatus disturbs the temperature rise at the center of the ring. As a consequence, the classical procedure used to identify the thermal conductivity of the material leads to noticeable errors. To overcome this difficulty, we proposed a modified identification procedure based on the numerical results computed with and without the slab of kapton, which permit to correct the influence of the thermal inertia of the apparatus. To use it successfully, it is only necessary to know the dimensions and properties of the kapton slab and the order of magnitude of the thermal properties of the material studied.

Secondly, we applied this modified identification procedure to several low-density EPS foams in order to determine whether the hot-ring technique could be extended to materials where radiative heat transfer also occurs. Indeed, the basic equation of the hot-ring method is rigorously only valid for purely conductive medium. The experimental and numerical results showed that when a perfectly emissive apparatus is used the thermal conductivity identified from the temperature rise is in good agreement with the equivalent thermal conductivity stemming from the guarded hot-plate method. We only observe small differences for the lighter foams ($\rho < 20\ \mathrm{kg\,m^{-3}}$) which do not behave as optically thick materials. The influence of the radiative heat transfer is then characterized by a slightly smaller value of the identified conductivity. However, even for extremely light foams ($\rho = 10\ \mathrm{kg\,m^{-3}}$), the relative difference remains always lower than 3%, which is lower than the measurement uncertainty of most of the other measuring techniques. On the other hand, for these non-optically thick foams, numerical investigations show that, when the apparatus (ring + kapton slab) is not perfectly emissive, the difference between the conductivity measured by the two methods reaches higher values which could no more be neglected. Fortunately, due to their composition (constantan and kapton), classical hot-ring apparatus could be considered as perfect emitters. Then, we can conclude that the hot-ring method based on the modified identification procedure could be extended to the low-density thermal insulators with an acceptable accuracy.

References

[1] H.P. Tan, B. Maestre, M. Lallemand, Transient and steady-state combined heat transfer in semi-transparent materials subjected to a pulse or a step irradiation, ASME J. Heat Transfer 113 (1) (1991) 166–173.
[2] O. Hahn, F. Raether, M.C. Arduini-Schuster, J. Fricke, Transient coupled conductive/radiative heat transfer in absorbing, emitting and scattering media: application to laser-Flash measurement on ceramic materials, Int. J. Heat Mass Transfer 40 (3) (1997) 689–698.
[3] M. Lazard, S. André, D. Maillet, Diffusivity measurement of semi-transparent media: model of the coupled transient heat transfer and experiments on glass, silica glass and zinc selenide, Int. J. Heat Mass Transfer 47 (2004) 477–487.
[4] B. Ladevie, Mise au point de dispositifs de caractérisation thermophysique de matériaux isolants solides ou pâteux. Extension aux fluides cisaillés, ENSAM Bordeaux, 1998.
[5] J.P. Laurent, Optimisation d'outils de mesure in situ des paramètres thermiques : Application au matériau TERRE, INPG Grenoble, 1986.
[6] R. Coquard, D. Baillis, D. Quenard, Experimental and theoretical study of the hot-wire method applied to low-density thermal insulators, Int. J. Heat Mass Transfer 49 (23–24) (2006) 4511–4524.
[7] R. Coquard, D. Baillis, Modeling of heat transfer in low-density EPS foams, J. Heat Transfer 128 (2006) 3279–3290.
[8] H.S. Carlslaw, J.C. Jaeger, Conduction of Heat in Solids, second ed., Oxford Univ. Press, Oxford, 1959.
[9] R. Siegel, J.R. Howell, Thermal Radiation Heat Transfer, third ed., Hemisphere Publishing Corp., Washington, DC, 1992.
[10] R. Viskanta, J. Lim, Transient cooling of a cylindrical glass gob, J. Quant. Spectrosc. Radiat. Transfer 73 (2002) 3279–3290.
[11] B.G. Carlson, K.D. Lathrop, Transport theory—the method of discrete ordinates, in: H. Greenspan, C.N. Kelber, D. Okrent (Eds.), Computing Methods in Reactor Physics, Gordon and Breach, New York, 1968, pp. 165–266.
[12] S. Jendoubi, H.S. Lee, T.-K. Kim, Discrete ordinates solution for radiatively participating media in a cylindrical enclosure, J. Thermophys. Heat Transfer 7 (1993) 213–219.
[13] M.Y. Kim, S.W. Baek, Modeling of radiative heat transfer in an axisymmetric cylindrical enclosure with participating medium, J. Quant. Spectrosc. Radiat. Transfer 90 (2005) 377–388.
[14] L.H. Liu, T. He-Ping, Transient radiation and conduction in a two-dimensional participating cylinder subjected to a pulse irradiation, Int. J. Thermal Sci. 40 (2001) 877–889.
[15] Wu, et al., Transient two dimensional radiative and conductive heat transfer in an axisymmetric medium, Heat Mass Transfer 33 (1998) 327–331.